ISSN 1560-8034, 1605-6582 (On-line), SPQEO, 2019. V. 22, N 2. P. 224-230.

Optics

Features of third-order optical nonlinearity in carbon disulfide

L.V. Poperenko, S.G. Rozouvan*

Taras Shevchenko Kyiv National University, Department of Physics
4, Glushkov Ave., 03022 Kyiv, Ukraine
**Corresponding author e-mail: sgr@univ.kiev.ua*

Abstract. Degenerate four-wave mixing (DFWM) processes in carbon disulfide have been experimentally studied applying the wavelength dependent femtosecond laser source. The quantum mechanical perturbation theory was applied to analyze the experimental data. Third-order optical nonlinearity in carbon disulfide has been proposed to consider two- or three-energy levels schemes. Either two-levels or three-levels scheme prevails in the nonlinear interaction depending on the symmetry of the participating in the interaction molecular orbitals. These two DFWM schemes have different spatial symmetry of three wave vectors of the laser beams, which leads to DFWM signal shape variation. Registered DFWM signals demonstrate the presence of a slow decay component for longer light wavelengths, which indicates availability of a virtual level in carbon disulfide having the same symmetry inherent to the ground state with 1.12 picoseconds lifetime. The DFWM signal shape based on symmetries of the carbon disulfide ground state and excited states has been analyzed. Quantum mechanics calculus was performed to build wave functions for the highest occupied (HOMO) and lowest unoccupied molecular orbitals (LUMO). Electronic states energies as well as optical transition energy for carbon disulfide were calculated with a few percents accuracy.

Keywords: third-order optical nonlinearity, carbon disulfide, perturbation theory, virtual levels.

https://doi.org/10.15407/spqeo22.02.224
PACS 31.15.xp, 42.65.An, 42.70.Nq, 82.53.Uv

Manuscript received 14.03.19; revised version received 05.05.19; accepted for publication 19.06.19; published online 27.06.19.

1. Introduction

Carbon disulfide plays a particular role in nonlinear optics experiments as a standard reference material. It is an easily available calibration sample with no absorption bands for popular laser wavelengths, which means constancy of its nonlinear numbers [1, 2]. Its simple chemical structure with double chemical bonds seems to be convenient to understand and demonstrate basic optical nonlinearity properties. However, carbon disulfide continues to be a subject of constant experimental efforts aimed at further studying its optical nonlinearity origin. The basic inspiration for these experiments is some gap between quantum-mechanical understanding of optical nonlinearity and practical aspects of construction of nonlinear optics based devices with extra large nonlinear electrical susceptibility tensor numbers. The basic quantum-mechanical perturbation theory cannot be applied directly to find a specific molecule among countless variety of chemical substances that must have a required nonlinear tensor. The molecule dipole optical transition moments cannot be presented as simple analytical expressions for a further analysis and can only be numerically evaluated using computer-based calculations, *e.g*., by applying molecular calculus [3] or Monte-Carlo approaches [4]. This gap between practical aspects and the theory limits further practical objectives of nonlinear optics, *e.g*., to synthesize a substance with considerably large nonlinear optical numbers [5]. From this viewpoint, all recent studies of carbon disulfide have one objective in common – to study further the optical nonlinearity fundamentals.

For example, the role of Raman scattering, two- and three-photon absorption in CS_2 nonlinearity was studied in [6, 7]. Fifth order processes and conditions when higher order processes exist were discussed in [7]. Particularities of real and imaginary parts of third-order nonlinear susceptibility as well as electron and nuclear contributions were studied in [8].

In [9], the authors tried to differ nonlinear properties of liquids and solids. Nonlinear coefficients of carbon disulfide were taken through microstructures of liquid phase, in particular, through correlation between nonlinear properties and different types of molecular arrangements of clusters surrounding CS_2 molecule. CS_2 nonlinear numbers were precisely determined using different approaches, namely: Z-scan, laser radiation and spectral shear interferometry [10, 11]. Molecular calculus was performed for determining electronic states, dipole moments and vibration frequencies of CS_2 [12].

The objective of this paper is to analyze the structure of third-order femtosecond nonlinear optical degenerate four-wave mixing (DFWM) signal from CS_2 by applying the fundamental principles of quantum-mechanical theory.

2. Theory

Nonlinear optical effects are associated with the terms of the expansion of induced polarization under influence of external light wave. Let us apply general time-dependent perturbation theory [13] for third-order nonlinear polarization of carbon disulfide in the DFWM case. The relationship for induced by three electric monochromatic fields $(\omega_p = \omega_q = \omega_r)$ $E_\beta \exp(-i\omega_p t)$, $E_\gamma \exp(-i\omega_q t)$, and $E_\eta \exp(-i\omega_r t)$ perturbation solution for the third order nonlinearity dipole moment:

$$\left\langle d_\alpha^{(3)} \right\rangle = \left(\frac{i}{\hbar}\right)^3 \int_{-\infty}^{t} dt_1 \int_{-\infty}^{t_1} dt_2 \int_{-\infty}^{t_2} dt_3$$
$$Sp\left\{\left[\left[d(t)_\alpha d(t_1)_\beta\right] d(t_2)_\gamma\right] d(t_3)_\eta\right\} E_\beta(t_1) E_\gamma(t_2) E_\eta(t_3). \quad (1)$$

Here, $d(t)_{\alpha(\beta,\gamma,\eta)}$ are electric dipole moment operators and α, β, γ, η indices responsible for light waves polarizations. Eq. (1) is derived by performing matrix density consecutive iterations $\rho(t) = \rho^{(0)} + \rho^{(1)}(t) + \rho^{(2)}(t) + ...$ which are the reaction of a system on perturbation Hamiltonian $V(t) = -dE(t)$. This Hamiltonian represents the time dependent interaction of the atom with an optical field in the dipole approximation (a light wave with instantaneous values of the electric field vector $E(t)$ that induces a dipole d). The upper limits of integration comply with causality principle constraints $t > t_1 > t_2 > t_3$. Integral in Eq. (1) is taken as a part of approach described in details in [14]. Classical representation of DFWM is two-level scheme (Fig. 1a), though from the viewpoint of perturbation theory approach we have to take into consideration all possible electronic transition schemes induced by three monochromatic waves. For example, the three-level scheme (Fig. 1b) satisfies Eq. (1) conditions, namely, each induced dipole moment arises as a result of an optical transition between two neighboring levels and interacts with a wave from three monochromatic waves.

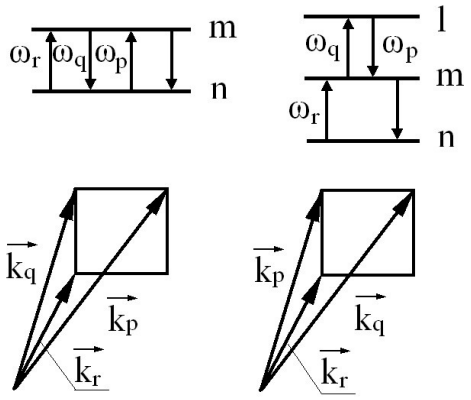

Fig. 1. DFWM in (a) two- and (b) three- energy level systems. Standing below are the wave vectors for mutual positions.

Having Eq. (1) integral, we can obtain a relationship for the three-level case. Here, all three light waves have the same frequencies (Fig. 1b), which means that we have third order nonlinearity in the DFWM scheme. The third-order nonlinear electrical susceptibilities coefficients may be derived as follows:

$$\chi(\omega,-\omega,\omega,-\omega)^{(3)}_{\alpha\beta\lambda\eta} = \frac{1}{2\hbar^3}$$
$$\sum_{\alpha\beta\lambda\eta=1,2,3} \left(\begin{array}{l} \dfrac{d_{nm}^{(\alpha)} d_{ml}^{(\beta)} d_{lm}^{(\gamma)} d_{mn}^{(\eta)}}{T_{mn}^{(3)} T_{ln}^{(2)} T_{mn}^{(1)}} - \dfrac{d_{nm}^{(\eta)} d_{ml}^{(\alpha)} d_{lm}^{(\beta)} d_{mn}^{(\gamma)}}{T_{nm}^{(3)} T_{mm}^{(2)} T_{lm}^{(1)}} + \\ + \dfrac{d_{nm}^{(\gamma)} d_{ml}^{(\beta)} d_{lm}^{(\alpha)} d_{mn}^{(\eta)}}{T_{ml}^{(3)} T_{mm}^{(2)} T_{mn}^{(1)}} - \dfrac{d_{nm}^{(\eta)} d_{ml}^{(\gamma)} d_{lm}^{(\beta)} d_{mn}^{(\alpha)}}{T_{nm}^{(3)} T_{nl}^{(2)} T_{nm}^{(1)}} - \\ - \dfrac{d_{nm}^{(\beta)} d_{ml}^{(\alpha)} d_{lm}^{(\gamma)} d_{mn}^{(\eta)}}{T_{lm}^{(3)} T_{ln}^{(2)} T_{mn}^{(1)}} + \dfrac{d_{nm}^{(\eta)} d_{ml}^{(\beta)} d_{lm}^{(\alpha)} d_{mn}^{(\gamma)}}{T_{nm}^{(3)} T_{nl}^{(2)} T_{lm}^{(1)}} - \\ - \dfrac{d_{nm}^{(\gamma)} d_{ml}^{(\alpha)} d_{lm}^{(\beta)} d_{mn}^{(\eta)}}{T_{ml}^{(3)} T_{ln}^{(2)} T_{mn}^{(1)}} + \dfrac{d_{nm}^{(\eta)} d_{ml}^{(\gamma)} d_{lm}^{(\alpha)} d_{mn}^{(\beta)}}{T_{nm}^{(3)} T_{nl}^{(2)} T_{ml}^{(1)}} \end{array} \right). \quad (2)$$

Here, $T_{ij}^{(3)} = \dfrac{1}{\omega_{ij} - 3\omega - i\gamma_{ij}}$, $T_{ij}^{(2)} = \dfrac{1}{\omega_{ij} - 2\omega - i\gamma_{ij}}$ and $T_{ij}^{(1)} = \dfrac{1}{\omega_{ij} - \omega - i\gamma_{ij}}$. γ_{ij} are damping terms. The tensor element represents the sum of all possible polarization indices commutations. Eq. (2) may be obtained using either Eq. (1) direct integration or simplifying the relationships for the third-order nonlinearity in the four-level scheme presented in [15] by reducing the number of levels from 4 down to 3. In the spectral region of two-photon absorption $\chi(\omega,-\omega,\omega,-\omega)^{(3)}_{\alpha\beta\lambda\eta}$ is equal to zero, because optical transitions with high value of transition cross section occur between even and odd orbitals (represented in Eq. (2) as n and l energy levels). In this case, the m level has either g or u symmetry, which means that either d_{nm}

or d_{ml} (which are presented in each component of Eq. (2)) is equal to zero, because the optical transition either between n and m levels or m and l levels is forbidden.

In frames of the two-level DFWM case (Fig. 1a), one can obtain a relationship for third-order optical nonlinearity $\chi(\omega,\omega,-\omega,-\omega)^{(3)}_{\alpha\beta\lambda\eta}$:

$$\chi(\omega,\omega,-\omega,-\omega)^{(3)}_{\alpha\beta\lambda\eta} = \frac{1}{2\hbar^3} \sum_{\alpha\beta\lambda\eta=1,2,3} \left(\begin{array}{l} \dfrac{d^{(\alpha)}_{nm} d^{(\beta)}_{mn} d^{(\gamma)}_{nm} d^{(\eta)}_{mn}}{T^{(3)}_{mn} T^{(2)}_{nn} T^{(1)}_{mn}} - \dfrac{d^{(\eta)}_{nm} d^{(\alpha)}_{mn} d^{(\beta)}_{nm} d^{(\gamma)}_{mn}}{T^{(3)}_{nm} T^{(2)}_{mm} T^{(1)}_{nm}} + \\ + \dfrac{d^{(\gamma)}_{nm} d^{(\beta)}_{mn} d^{(\alpha)}_{nm} d^{(\eta)}_{mn}}{T^{(3)}_{mn} T^{(2)}_{mm} T^{(1)}_{mn}} - \dfrac{d^{(\eta)}_{nm} d^{(\gamma)}_{mn} d^{(\beta)}_{nm} d^{(\alpha)}_{mn}}{T^{(3)}_{nm} T^{(2)}_{nn} T^{(1)}_{nm}} - \\ - \dfrac{d^{(\beta)}_{nm} d^{(\alpha)}_{mn} d^{(\gamma)}_{nm} d^{(\eta)}_{mn}}{T^{(3)}_{nm} T^{(2)}_{nn} T^{(1)}_{mn}} + \dfrac{d^{(\eta)}_{nm} d^{(\beta)}_{mn} d^{(\alpha)}_{nm} d^{(\gamma)}_{mn}}{T^{(3)}_{nm} T^{(2)}_{nm} T^{(1)}_{nm}} - \\ - \dfrac{d^{(\gamma)}_{nm} d^{(\alpha)}_{mn} d^{(\beta)}_{nm} d^{(\eta)}_{mn}}{T^{(3)}_{mn} T^{(2)}_{mn} T^{(1)}_{mn}} + \dfrac{d^{(\eta)}_{nm} d^{(\gamma)}_{mn} d^{(\alpha)}_{nm} d^{(\beta)}_{mn}}{T^{(3)}_{nm} T^{(2)}_{nn} T^{(1)}_{mn}} \end{array} \right). \quad (3)$$

Eq. (3) may be directly derived from Eq. (2) by substitution $l = n$.

3. Experiment and discussion

The set-up that we used in order to perform spectral DFWM was described in details in [16-18]. To perform optical wavelength tuning the femtosecond pulses, a light source consisting of a femtosecond Ti/sapphire oscillator (Coherent Mira 900F), a regenerative Ti/sapphire amplifier (Coherent RegA 9000), and an optical parametric amplifier (OPA) (Coherent 9400) was used. This produced 170 femtosecond pulses were tunable in a broad spectral range, including the wavelength interval from 500 to 700 nm. The repetition rate was 150 kHz, allowing effective lock-in detection in order to improve the signal-to-noise ratio of the DFWM signal in the folded box coherent anti-Stocks Raman scattering (CARS) configuration without generating thermo-optical effects. The three collinear beams (one is with a tunable temporal delay) were focused onto the same sample spot by a lens with 100 mm focal length, leading to a focal diameter approximately of 20 μm. The fourth deflected beam as the studied DFWM signal was detected by a silicon photodiode (Hamamatsu followed by a Stanford Research preamplifier SR 620). Lock-in techniques (Stanford Research SR530) were used to improve the signal-to-noise ratio of the DFWM signal. Two of these incoming beams were chopped by a mechanical chopper at different frequencies, and the signal was detected at the frequency sum.

CS_2 liquid was used by us as a reference sample in numerous spectral DFWM experiments [16-18]. A huge amount of these data as well as additional measurements performed for CS_2 sample have confirmed existence of DFWM signal profile development in 600-nm spectral region. Our measurements of the DFWM response from carbon disulfide in 600-nm spectral region found three distinct components of the signal having different progress in time. Fig. 2 curves maxima are located in 170 femtoseconds interval which is within OPA pulse duration. Here, we can put emphasis on distinct spectral nonlinearity dynamics. The fast component that is usually called as a "coherent artifact" is basically DFWM signal either in the two- or three-level scheme. For the three-level scheme, the DFWM signal maximum arises by 150 fs later. Longer wavelength signals maxima are delayed as compared to DFWM signals induced by shorter wavelength light.

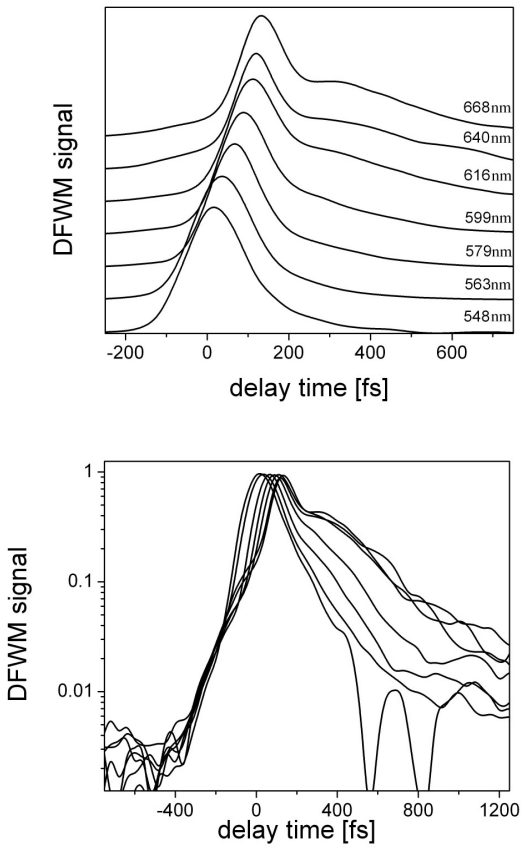

Fig. 2. DFWM signal in carbon disulfide at various wavelengths (a) as 3D graph (the curves are gradually shifted in vertical direction), (b) in logarithmic scale.

DFWM for two- and three-energy levels.

In two-photon absorption spectral interval (~600 nm)	DFWM in the two-level scheme, slow decay component is not presented	n(HOMO) – odd (/even), m(virtual state) – even (/odd), l(LUMO) – even (/odd)
Outside two-photon absorption spectral interval	DFWM in the three-level scheme, slow decay component is presented	n(HOMO) – odd (/even), m(virtual state) – even (/odd), l(virtual state) – odd (/even)

Note. HOMO – highest occupied and LUMO – lowest unoccupied molecular orbitals.

In Table, the basic features in these two different cases, namely, for two-photon spectral absorption region and for a non-resonant spectral interval outside the two-photon absorption band are presented. The three-level scheme DFWM signal disappears for the wavelengths within two-photon absorption transition spectral interval, because of the different symmetry for ground and the upper excited state with zero dipole moment between the intermediate level and one of two other energy states (two levels from *n*, *m* and *l* energy levels from Eq. (2) have the same symmetry). The two- and three-level schemes that form third-order nonlinear dipole are simultaneously allowed by symmetry rules (in visible and near infrared regions below two-photon absorption bands), but only one three-level scheme is responsible for curves with the delayed maximum and slow decay components from Fig. 2. It means that nonzero third-order nonlinearities cannot exist simultaneously in the two- and three-energy level schemes either because of spatial symmetry restrictions or by another reason. Let us consider the latter moment in details.

In Fig. 2, curves maxima shift gradually with lasing light wavelengths. Eq. (1) is invariant in respect to commutations of β, γ, and η indices and as a result the third-order nonlinear tensor for isotropic media is commutatively invariant. Technically, commutative symmetry is valid for paraxial monochromatic waves, and it was experimentally confirmed in [16]. If the paraxial approximation is not well satisfying, three laser beams no longer may be taken as equivalent ones. For our case of Fig. 2, maxima temporal shifts can be considered as a result of commutative symmetry violation. Commutative symmetry is violated because of non-equivalence of three beams from the viewpoint of DFWM geometries for two- (Fig. 1a) and three-level (Fig. 1b) schemes. It may result it DFWM signal maxima shift. For example, if one takes three pulses delayed in time (Fig. 3), then it gives the maximum nonlinear signal based on Eq. (1) scheme. The causality principle is presented in Eq. (1) as upper limits of integration – each consecutive pulse affects the system after an influence of electric field from the previous laser pulse. So, if we for example decide to exchange the places of the pulses that propagate along t_1 and t_3 axes in Fig. 3b, the resulted third-order nonlinear dipole will be extremely small, because the third wave that must interact with dipoles induced by the first two waves is almost passed through the volume of three beams convergence. The timing orders of interaction of all three beams are reflected in Fig. 1 geometries that are different for two- and three-level schemes. The shift of t_2 pulse (which is visible in Fig. 2 as curves maxima shifts) allows us to apply Fig. 1a for DFWM in the three-level schemes, too. In this case, relationships for wave vectors for the two- (upper relationship) and three-level (bottom relationship) schemes are still valid:

$$\vec{k}_r - \vec{k}_q + \vec{k}_p - \vec{k}_{signal} = 0,$$
$$\vec{k}_r + \vec{k}_p - \vec{k}_q - \vec{k}_{signal} = 0. \qquad (4)$$

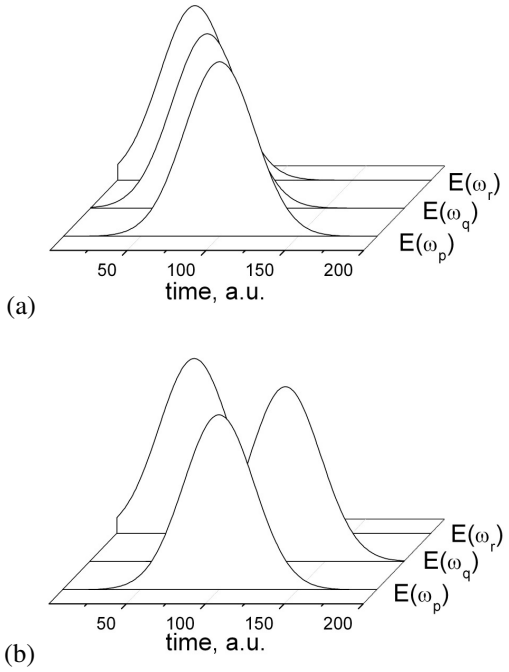

Fig. 3. Pulses mutual temporal arrangement for the (a) two- and (b) three-level schemes.

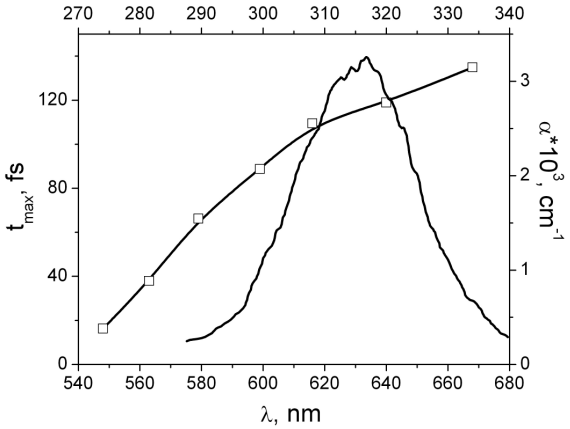

Fig. 4. Position of DFWM signals maxima as a function of wavelength (the left and bottom axes). Carbon disulfide absorption as a function of wavelength (the right and upper axes).

Here, the different order of wave vectors subscript indices reflects Eq. (1) both causality principle and commutation symmetry. Two different subscript indices commutations are present in Eq. (4) – (r,q,p) and (r,p,q). The latter commutation arises as time delay of $E(\omega_p)$ beam, which is visible in Fig. 2 as curves maxima delays as a function of wavelength. Slow decay components are unexpectedly present in Fig. 2 nonlinear signal curves, though usually it exist in substances with strong absorption bands due to induced excited states population gratings. In these schemes, the weak slow decay component (time constant t_{vl} = 1.12 picoseconds) is

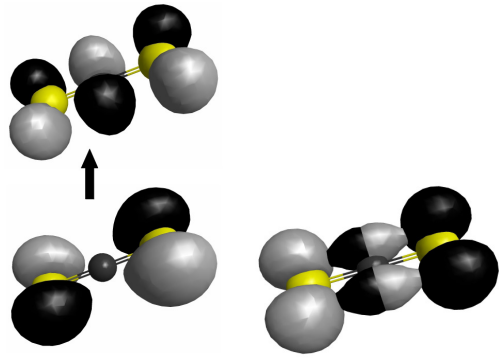

a b

Fig. 5. Calculated wave functions for CS_2 molecule. (a) wave functions density (isovalue 0.05) for HOMO (below) and LUMO molecular orbitals, (b) wave functions density (isovalue 0.01) for the mixed wave function (optical transition between HOMO and LUMO orbitals).

diffraction of a delayed third beam on population grating formed by two beams [17], similarly to DFWM in optical absorption spectral interval. But in our case, the grating is formed by two-photon absorption on a virtual level with forbidden one-photon transition to the ground state. We can only speculate about the origin of the virtual levels, though it may be related to unpopulated electron-vibrational levels [19]. Parameter t_{vl} is a few orders of magnitude less than electronic excited states lifetimes though it is registered in DFWM setup with 0.1% measurement error (Fig. 2b). Basically, our experience shows that the very weak slow decay component is always present in carbon disulfide within 0.7…1.4 μm spectral interval. As we can see, the quasi-stable virtual level in carbon disulfide has a measurable lifetime in strong light field and therefore may be related to low populated electron-vibrational level with the energy gap relatively to HOMO state, which matches the laser light frequency. We measured 317 nm CS_2 absorption band by using the Hitachi U-3900/3900H spectrophotometer and a cuvette with a few tens micrometers thickness. The CS_2 absorption peak and DFWM signal maxima are presented in Fig. 4. We can see time evolution of DFWM signal, which is noticeably correlated to CS_2 absorption band in the doubled optical frequency spectral interval.

The 1.12 picosecond slow decay component indicates on quasi-stable virtual level *l* which appears as a result of DFWM interaction in CS_2 nonresonant spectral region. This level with relatively low (comparing to virtual level *m*) dumping term is responsible for resonant enhancement of nonlinear dipole induced in the three-level scheme comparing to the two-level scheme case. The enchancement is a result of low denominators in Eq. (1) terms $T_{lm}^{(1)} = \dfrac{1}{\omega_{lm} - \omega - i\gamma_{lm}}$ because of relatively stable upper virtual level *m* in the three-level scheme and relatively small dumping terms γ_{lm}. The denominators in the relevant terms for the two-level case are higher, because of the negligibly small virtual level lifetimes. If trying to analyze Fig. 2b signal behavior, one can see smooth rise in the slow decay component intensity as well as evolution of curves maximum positions as a function of wavelength numbers. It means that three-level DFWM have a higher efficiency as compared to the two-level scheme in the nonresonant region. The position of two-photon absorption line in the 630-nm spectral region marks the boundary between these two DFWM schemes. The curves from Fig. 2a are normalized taking into account the photodiode due to experimental setup spectral sensitivity, which indicates constant CS_2 third-order nonlinearity numbers in the 548…668-nm spectral range. We believe that the constancy of the nonlinearity tensor independently of two different energy level schemes indicates existence of a more general equation for optical nonlinearity that should include Eqs. (1), (2) as invariant forms.

To illustrate these considerations, we have performed molecular calculus on carbon disulfide molecule by applying excitation energies in the frame of TD-DFT (Time-Dependent Density Functional Theory) approach by using GAMESS software [20]. The energy of the lowest dipole transition was determined in our calculations as 4.159 eV (which corresponds to the wavelength of 298.11 nm). The results of numerical calculations are in sufficiently good correlation with the measured CS_2 absorption peak position (Fig. 4). Spatial distributions of electron density in the ground and excited states are presented in Fig. 5. The distributions for LOMO and HUMO molecular orbitals are typical for these linear three-atomic molecules [21]. We have also presented the mixed state electron density distributions for the case $(\varphi_l - \varphi_n)^2$ and $(\varphi_l + \varphi_n)^2$, which illustrate the density in times 0 and *T*/2 (*T* is the period of oscillation with Bohr frequency $\hbar\omega_{nl}$) depicted in grey and black colors. They form a dipole that arises during optical transition in dipole approximation.

The transition seems to be identified earlier [22] as a transition between $^1\Delta_u$ and $^1\Sigma_g^+$ energy levels, though it was determined as being complex and not well understood. Detailed studies of CS_2 spectrum [23] revealed this region absorption band contains five different bands related to different equilibrium geometries of CS_2 molecule.

4. Conclusions

In this paper, we have presented the data on spectral evolution of third-order nonlinear properties inherent to carbon disulfide. The degenerate four-wave mixing experiments were performed with visible wavelengths femtosecond laser pulses and were analyzed applying general time-dependent perturbation theory. The major points of our research are summarized below.

1. We proposed to consider degenerate four-wave mixing interaction as a process with four optical transitions of the same frequency in two basic schemes, namely, with three or two energy levels. These two

presented schemes are a consequence of probabilistic nature of quantum mechanics, and we have to take into account all possible transitions induced by monochromatic laser light.

2. Two- and three-level DFWM interactions have different cross-sections and basically cannot be active simultaneously. The efficiency of each scheme depends on symmetry of the molecular orbitals participating in the interaction. The presence of absorption bands and the two-photon ones influences the symmetry of electron and virtual DFWM energy levels and make then a specific DFWM format to be active or nonactive in some spectral interval.

3. Two- and three-level DFWM interactions have different spatial symmetry of their wave vectors, which results in DFWM signal shape variation due to causality principle for three interacting light waves.

4. Carbon disulfide exhibits the presence of virtual levels with relatively high lifetimes of 1.12 picoseconds, which are responsible for the existence of slow decay component in the DFWM signals. The slow decaying part of DFWM signal is a result of third delayed beam diffraction on a population grating. The grating that is noticeable in the femtosecond time scale appears because of a populated virtual level having the same symmetry as the ground state. The intensity of the slow component is relatively low as compared to the DFWM signal at its maximum, because of low numbers for two-photon transition cross-sections.

5. Carbon disulfide demonstrates constancy of its third-order nonlinearity numbers despite distinct variations in DFWM specifics across the broad spectral range. From our viewpoint, it indicates the possibility of some integral solution for optical nonlinearities, which should include particular solutions of general time-dependent perturbation theory as its parts.

Molecular calculus has allowed to receive numerical solution for time-independent Schroedinger equation, which illustrates coincidence of the theory approach and the experimental results. The approach may be proposed in order to analyze the spectral femtosecond DFWM data for broad variety of substances.

References

1. Boudebs G. and Fedus K. Absolute measurement of the nonlinear refractive indices of reference materials. *J. Appl. Phys.* 2009. **105**. 103106 (5p). https://doi.org/10.1063/1.3129680.
2. Ganeev R.A., Ryasnyanskii A.I., and Kuroda H. Nonlinear Optical Characteristics of Carbon Disulfide. *Optics and Spectroscopy*. 2006. **100**, No. 1. P. 108–118. https://doi.org/10.1134/S0030400X0601019X.
3. Fripiat J.G., Barbier C., Bodart V.P., and Andre J.M. Calculations of first- and second-order nonlinear molecular hyperpolarizabilities by perturbation methods: I. An efficient method for evaluating time-independent hyperpolarizabilities. *J. Comput. Chem*. 1986. **7**, No. 6. P. 756–760. https://doi.org/10.1002/jcc.540070608.
4. Shafei S., Kuzyk M.C., and Kuzyk M.G. Monte-Carlo studies of the intrinsic second hyperpolarizability. *J. Opt. Soc. Am. B.* 2010. **27**, No. 9. P. 1849–1856. https://doi.org/10.1364/JOSAB.27.001849.
5. Lytel R. Physics of the fundamental limits of nonlinear optics: a theoretical perspective [Invited]. *J. Opt. Soc. Am. B.* 2016. **33**, No. 12. P. E66–E82. https://doi.org/10.1364/JOSAB.33.000E66.
6. Yan X.-Q., Liu Z.-B., Shi S. et al. Analysis on the origin of the ultrafast optical nonlinearity of carbon disulfide around 800 nm. *Opt. Exp.* 2010. **18**, No. 25. P. 26169–26174. https://doi.org/10.1364/OE.18.026169.
7. Kong D. G., Chang Q., Ye H. *et al*. The fifth-order nonlinearity of CS_2. *Journal of Physics B: Atomic, Molecular and Optical Physics.* 2009. **42**. 065401 (4 p). https://doi.org/10.1088/0953-4075/42/6/065401.
8. Yan X.-Q., Zhang X.-L., Shi S. et al. Third-order nonlinear susceptibility tensor elements of CS_2 at femtosecond time scale. *Opt. Exp*. 2011. **19**, No. 6. P. 5559–5564. https://doi.org/10.1364/OE.19.005559.
9. Li W., Tian W. Q., and Sun X. Understanding of nonlinear optical properties of CS_2 from a microscopic viewpoint. *J. Chem. Phys.* 2012. **137**. 084315 (7 p.). https://doi.org/10.1063/1.4748261.
10. Couris S., Renard M., Faucher O., Lavorel B., Chaux R., Koudoumas E., Michaut X. An experimental investigation of the nonlinear refractive index (n_2) of carbon disulfide and toluene by spectral shearing interferometry and *z*-scan techniques. *Chem. Phys. Lett.* 2003. **369**. P. 318–324. https://doi.org/10.1016/S0009-2614(02)02021-3.
11. Ganeev R.A., Ryasnyansky A.I., Baba M., Suzuki M., Ishizawa N., Turu M., Sakakibara S., Kuroda H. Nonlinear refraction in CS_2. *Appl. Phys. B.* 2004. **78**. P. 433–438. https://doi.org/10.1007/s00340-003-1389-y.
12. Tseng D.C. and Poshusta R.D. *Ab initio* potential energy curves for low-lying states of carbon disulfide. *J. Chem. Phys.* 1994. **100**. P. 7481–7486. https://doi.org/10.1063/1.466892.
13. Orr B.J. & Ward J.F. Perturbation theory of the non-linear optical polarization of an isolated system. *Molecular Physics – An International Journal at the Interface between Chemistry and Physics*. 1971. **20**, No. 3. P. 513–526. https://doi.org/10.1080/00268977100100481.
14. Yariv A. The application of time evolution operators and Feynman diagrams to nonlinear optics. *IEEE Journal of Quantum Electronics*. 1977. **QE-13**, No. 12. P. 943–950. https://doi.org/10.1109/JQE.1977.1069267.
15. Prior Y. A complete expression for the third-order susceptibility ($\chi^{(3)}$) – Perturbative and Diagrammatic Approaches. *IEEE Journal of Quantum Electronics*. 1984. **QE-20**, No. 1. P. 37–42. https://doi.org/ 10.1109/JQE.1984.1072262.

16. Rozouvan S. Commutative spatial and time symmetry of degenerate four-wave mixing measurements. *J. Opt. Soc. Am. B: Opt. Phys.* 1999. **16**, No. 5. P. 768–773. https://doi.org/10.1364/JOSAB.16.000768.
17. Rozouvan S. Broadband degenerate four-wave-mixing measurements. *J. Opt. Soc. Am. B: Opt. Phys.* 2000. **17**. No. 8. P. 1354–1359. https://doi.org/10.1364/JOSAB.17.001354.
18. Schrof W., Andreaus R., Moehwald H., Rozouvan S., Belov V., Van Keuren E., and Wakebe T. Nonlinear optics of polythiophene films. *Molecular Crystals and Liquid Crystals Science and Technology Section B: Nonlinear Optics.* 1999. **22**(1–4). P. 295–300.
19. Bahaa E. A. Saleh, Bradley M. Jost, Hong-Bing Fei, and Malvin C. Teich entangled-photon virtual-state spectroscopy. *Phys. Rev. Lett.* 1998. **80**, No. 16. P. 3483–3486. https://doi.org/10.1103/PhysRevLett.80.3483.
20. Schmidt M.W., Baldridge K.K., Boatz J.A. *et al.* General atomic and molecular electronic structure system. *J. Comput. Chem.* 1993. **14**. P. 1347–1363. https://doi.org/10.1002/jcc.540141112.
21. Griffith J.S. and Orgel L.E. Ligand-field theory. *Quarterly Reviews, Chemical Society.* 1957. **11**. P. 381–393.
22. McGlynn S.P., Rabalais J.W., McDonald J.R., and Scherr V.M. Electronic spectroscopy of isoelectronic molecules. II. Linear triatomic groupings containing sixteen valence electrons. *Chem. Rev*. 1971. **71**, No. 1. P. 73–108. https://doi.org/10.1021/cr60269a004.
23. Zhang Q. and Vaccaro P.H. *Ab initio* studies of electronically excited carbon disulfide. *J. Phys. Chem.* 1995. 99, No. 6. P. 1799–1813. https://doi.org/10.1021/j100006a024.

Authors and CV

Leonid Poperenko, born in 1950, defended his Doctoral Dissertation in Physics and Mathematics in 1992 and became full professor in 1996. Head of Department of Optics at the Taras Shevchenko National University of Kyiv. Authored over 200 publications, 15 patents, 7 textbooks. The area of his scientific interests includes spectral ellipsometry of metals and surface science.

Stanislav Rozouvan, born in 1961, defended his PhD thesis in optics and laser physics in 1995. Scientist at the Department of Optics of Taras Shevchenko National University of Kyiv. Authored over 70 publications, 3 patents. The area of his scientific interests includes scanning tunneling microscopy and third-order nonlinear optics.